The Cryosphere, 5, 329–340, 2011
www.the-cryosphere.net/5/329/2011/
doi:10.5194/tc-5-329-2011

The Cryosphere

Imaging the structure of cave ice by ground-penetrating radar

H. Hausmann and M. Behm

Institute of Geodesy and Geophysics, Vienna University of Technology, Austria

Received: 14 August 2010 – Published in The Cryosphere Discuss.: 23 August 2010
Revised: 22 March 2011 – Accepted: 6 April 2011 – Published: 13 April 2011

Abstract. Several caves in high elevated alpine regions host up to several meters thick ice. The age of the ice may exceed some hundreds or thousands of years. However, structure, formation and development of the ice are not fully understood and are subject to relatively recent investigation. The application of ground-penetrating radar (GPR) enables to determine thickness, volume, basal and internal structure of the ice and provides as such important constraints for related studies. We present results from four caves located in the Northern Calcareous Alps of Austria.

We show that the ice is far from being uniform. The base has variable reflection signatures, which is related to the type and size of underlying debris. The internal structure of the cave ice is characterized by banded reflections. These reflection signatures are interpreted as thin layers of sediments and might help to understand the ice formation by representing isochrones. Overall, the relatively low electromagnetic wave speed suggests that the ice is temperate, and that a liquid water content of about 2% is distributed homogenously in the ice.

1 Introduction

Ice caves ("Eishöhle" in german) are natural cavities with the occurrence of ice which persists for at least several years. Age, formation, development, conservation and degradation of the "underground ice" attracted scientific interest since the beginning of the 20th century and are also subject to relatively recent investigation (Luetscher, 2005, and references within). In 2006 a pilot study (AUSTRO*ICE*CAVES*2100) has been started to encompass the above mentioned topics and primarily aims to fortify the basics and fundamental knowledge on ice caves. This includes the link between (Speleo-) meteorology and ice formation, determining the age of the ice as well as local quantification of ice volumes. Additionally, in regard of the current climate debates, the ice caves' potential as possible climate archives should be investigated. The presented GPR data have been acquired in this project.

Based on the fact that the ice exists for at least several years, it can be classified as a permafrost phenomenon. The application of geophysical methods to study glacial or frozen materials depends on the physical properties of earth materials which change with freezing of incorporated water and therefore the formation of varying amounts of ground ice. The relevant electric parameters are resistivity (real- or complex-valued), relative permittivity, and loss tangent (Scott et al., 1990). Variation in these physical properties depends on liquid water content, air content, ice chemistry, and temperature conditions during permafrost genesis. EM (electrical and electromagnetic) techniques that operate at frequencies of a few Hz (e.g. D.C. resistivity sounding) are sensitive to the resistivity of materials whereas frequencies >100 kHz (e.g. GPR) are influenced by both resistivity and relative permittivity (Katsube et al., 1976). In this study, we show that GPR can be successfully used to map the thickness and structure of the ice. Cave ice thickness measurements with GPR have also been carried out in the Dobsinska ice cave (Slovakia) (Geczy and Kucharovic, 1995; Novotny and Tulis, 1995) and in Kungur ice cave (Russia) (Podsuhin and Stepanov, 2008).

In this study we document the internal and basal structure of the ice in four different caves and highlight their pronounced differences. Therefore we apply uniform and additional processing techniques (migration) to the GPR data, and focus on the internal ice structure and the associated reflection signatures. We further investigate particular features such as layering of the ice and relate them to the formation of ice.

Correspondence to: H. Hausmann
(hausmann@mail.zserv.tuwien.ac.at)

Published by Copernicus Publications on behalf of the European Geosciences Union.

2 Ice caves

Occurrence of ice in caves results mainly from water which enters through the porous rock. If the temperature is below zero, ice starts to form. Due to isolation by the surrounding rocks, the air temperature inside a cave is rather constant throughout the year. It equals to the annual average of the outside air temperature and therefore depends mainly on the elevation and geographic region. Additionally, most caves have more than one entrance and are ventilated. In summer, the relatively cold and dense cave air sinks down and flows out at the lower entrances. In winter, this regime changes and relatively warm cave air of lower density leaves through the upper entrances. For compensation, cold outside air is sucked into the cave at the lower entrances (Cigna, 2004). Ice grows therefore close to the lower entrances in winter and early spring when the outside temperature still is low and water enters the cave. On the other hand, the ice degrades in summer and autumn. Recent investigations (Delaloye and Lambiel, 2005; Phillips et al., 2009) found that the formation of ice in ventilated talus slopes is controlled by a similar effect.

Heat exchange with the surrounding rock and air, and sublimation are other factors controlling the dynamic behaviour of the ice (Yonge, 2004). It is obvious that growth and degradation are very sensitive to (micro-) climatic changes. Ice caves can be considered as environmental markers as the presence of ice is controlled by specific climatic conditions (e.g. winter precipitation, number of freezing days, mean annual air temperature; Luetscher, 2005). Nonlinear effects also play important roles: e.g., some entrances may be blocked by ice for a certain time and their opening changes the ventilation which in turn leads to ice growth and blockage of other entrances (Wimmer, 2008). Despite these various influences, we know from direct observation that massive ice bodies can pertain for at least hundred years. Dating of organic inclusions in ice caves yields ages up to 5180 ($\pm$130) years (Achleitner, 1995). It is important to stress out the difference between seasonal ice (which completely disappears in summer and autumn and starts to form again in winter) and occurrences of ice bodies which exist for at least several years. We only deal with the latter permafrost feature in this study.

Approximately 13 000 caves are currently known in the Northern Calcareous Alps and about 900 of them comprise ice (Stummer and Plan, 2002). On average, the ice-filled parts are located in elevations ranging from 1300 to 2000 m a.s.l. We investigate the ice of four caves (Fig. 1): Eisriesenwelt, Dachstein-Mammuthöhle, Dachstein-Rieseneishöhle and Beilstein-Eishöhle. For the first three caves, detailed descriptions of the field measurements and initial results (thickness) have already been published by Behm and Hausmann (2007, 2008).

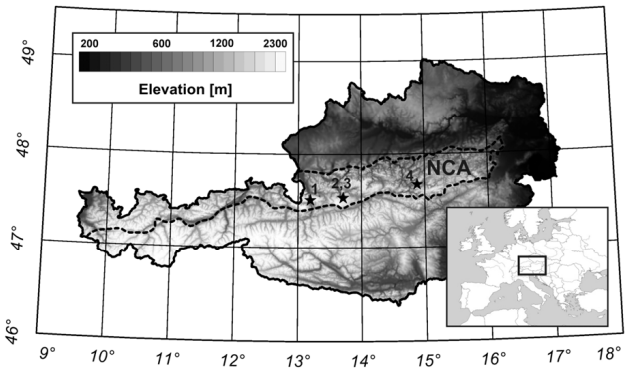

Fig. 1. Location of the investigated caves: 1 – Eisriesenwelt; 2, 3 – Dachstein-Mammuthöhle, Dachstein-Rieseneishöhle; 4 – Beilstein-Eishöhle. The broken line displayed over the digital elevation model encompasses the Northern Calcareous Alps (NCA).

3 Method

Ground-penetrating radar (GPR) is a geophysical method based on the propagation and reflection of electromagnetic waves (Davies and Annan, 1989) in the radio band. A short electromagnetic pulse of suitable frequency is radiated and the propagating wave is partially reflected when permittivity and/or conductivity inside the medium changes. Such a change is either a first-order discontinuity (e.g. an air void) or a zone with a strong gradient (e.g. continuously increasing pore space) (Robin et al., 1969). The reflected energy from the pulse is recorded as a function (amplitude and phase) of time, in form of a single trace. A radargram is made up of several traces, where the traces are recorded on adjacent surface locations along a profile. If the electromagnetic wave speed of the medium is known, the correct position of subsurface reflectors can be imaged ("migration"). This method is commonly employed to investigate the structure of the shallow underground. Since the 1960s GPR is applied as a method for locating and mapping subglacial interfaces, and thereby to constrain ice volume and morphology (e.g. Robin et al., 1969; Arcone et al., 1995; Binder et al., 2009). Changes in crystal-orientation fabric, changes in conductivity or changes in the amount of bubbles (respectively density) are considered to cause internal reflections in glaciers and ice sheets (e.g. Harrison, 1973; Gudmandsen, 1975; Siegert, 1999; Eisen et al., 2007). Strong internal and basal reflectors can further be caused by layers of varying density within firn and snow (Bingham and Siegert, 2007), sediments (Woodward et al., 2003), debris (Arcone et al., 1995; Fukui et al., 2008) or subglacial lakes.

We used the GSSI SIR 2000 and 3000 instruments with shielded antennas ranging from 200 to 500 MHz. Most of the measurements were obtained from the 500 MHz antenna. However, in one of the caves (Dachstein-Rieseneishöhle), larger depths were expected and therefore a

shielded 200 MHz antenna was applied. The measurements were carried out along crossing profiles in a time-based data collection mode. As 32 traces per second were recorded, the lateral trace spacing depends on the speed by which the antenna is moved along the ground. On average it was about 0.025 m.

Marks at an interval of 2 m (using a measuring tape) were added to the recordings to obtain precise positions. We estimate the positioning accuracy of the collected traces to be ± 0.02 m per marker interval (2 m).

Since almost all profiles were obtained on planar surfaces, their geometry could be defined with a geodetic measuring tape. However, for profile "Feenpalast 2" we surveyed the position of significant changes in the profile height with simple geodetic methods (laser distance meter and inclinometer). Taking the expected depths into account, the record lengths ranged between 100 and 400 ns. An electromagnetic pulse of 500 MHz propagates with a wavelength of 0.33 m in ice, which results in a vertical resolution of about 0.08 m (1/4 of the signal wavelength (Yilmaz, 2001). It should be mentioned that a lower resolution is obtained when the length of the wavelet is considered instead of the wavelength (e.g. Eisen et. al., 2002). Recording parameters of each trace were 2048 samples/scan and 16 bits/sample. Spatially equidistant traces were interpolated for each radargram for intervals of 0.025 m. The horizontal resolution is a function of depth and the wavelength and is defined by the first Fresnel zone (Yilmaz, 2001). For a investigation depth of 5 m and an electromagnetic wave speed of 0.167 m ns^{-1} the Fresnel zone has a diameter of 1.8 m (500 MHz) and 2.9 m (200 MHz).

The raw data were processed with trace mixing (reduction of antenna noise), automatic gain control (15 ns length), trapezoid band pass-filter for the 500 MHz records (250-350-700-900 MHz) and 200 MHz records (50-100-400-600 MHz), migration (including velocity analyses), and static corrections using the 2-D software ProMAX (Landmark). For the migration we applied the Steep dip explicit FD time migration algorithm with a maximum dip of 50°. Electromagnetic wave speed was assessed by both reflection hyperbolae identified in numerous radargram sections and migration velocity analyses. It has to be pointed out that the use of shielded antennae was crucial since the surrounding walls of the caves are strong reflectors. All discussed features were carefully examined with regard to their possible origins. Since we focus on the documentation and comparison of different locations, the presented radargrams are consistently processed. In the following we show both the unmigrated and migrated radargrams, and highlight details of characteristic internal and basal structures.

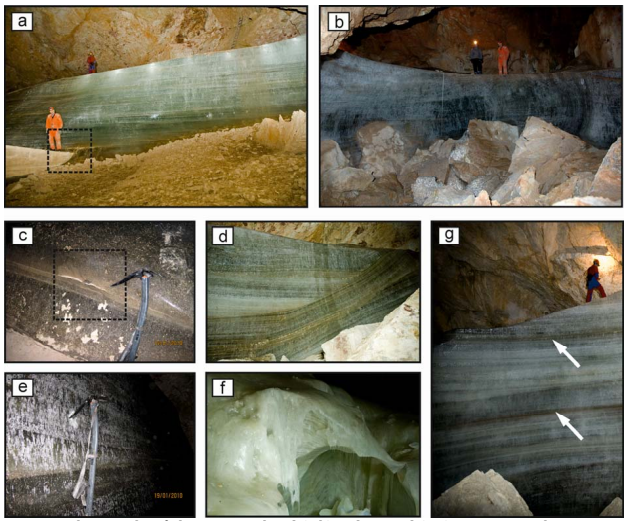

Fig. 2. Photographs of characteristic basal **(a–b)** and internal **(c-g)** structures in the ice caves **(a)** The ice at "Feenpalast 1" (Dachstein-Mammuthöhle) with an interbedded boulder. The basal substrate consist of fine-grained sediments. **(b)** The ice at "Saarhalle" (Dachstein-Mammuthöhle) with large boulders on the base. **(c)** The diaphanous ice at "Feenpalast 1" with embedded thin layers of accumulated particles. A zone of high particle density is highlighted. **(d)** Subsurface parallel strata in the footwall and horizontal strata in the hanging wall found at "Feenpalast 2". **(e)** Detail of the diaphanous ice shown in a). Slight stratification is indicated by a variable content of millimetre-sized bubbles and a low amount of embedded particles. **(f)** The intransparent ice at Dachstein-Rieseneishöhle with a hole (diameter ∼2 m) which has been formed by air currents. **(g)** Side view of the intransparent ice at "Feenpalast 2" and two sediment layers which are also seen as reflection bands in the radargram (Fig. 3d).

4 Field sites

4.1 Dachstein-Mammuthöhle

Dachstein-Mammuthöhle has an overall passage length of 65 km and a vertical extension of 1207 m. Ice occurrences are located close to the western entrance, which is situated 800 m below the currently known highest entrances. At "Feenpalast" (1360 m a.s.l.) two locations with ice can be found. The location "Feenpalast 1" is dominated by a 25 m × 10 m wide and 3 to 4 m thick ice block (Fig. 2a) which is relatively homogenous, and appears clear and diaphanous (Fig. 2e). Only a slight stratification is indicated by a variable content of millimetre-sized bubbles. The amount of embedded particles is generally low. However, layers with different grades of dispersal can still be discriminated. The base consists of frozen clay and debris with a grain size of a few centimetres. A 17 m long profile was measured on top of the ice. Temperature measurements during the GPR campaign in January 2008 show that the lowermost temperature is obtained at the ice surface (−2.7 °C). Temperature

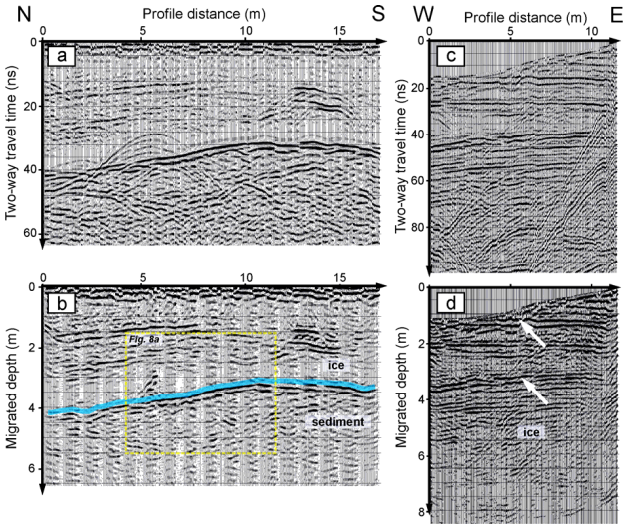

Fig. 3. Radargram sections of the ice at "Feenpalast 1" (Fig. 2a) and "Feenpalast 2" (Fig. 2g) (Dachstein-Mammuthöhle). **(a, b)** The fairly diaphanous ice clearly exhibits the transition from ice to the fine-grained sediment. The blue line in the migrated section **(b)** shows the base. **(c, d)** Radargram sections of the intransparent ice with strata found close to the previous location. Arrows indicate the layers which are also seen on the side of the ice cliff (Fig. 2g)

measurements in 0.08 m depth of the ice yield values of $-1\,^{\circ}$C in the bottom part and $-0.4\,^{\circ}$C at the base. In general liquid water could be observed at the surface of all ice locations (in autumn), but was never encountered at the base. However, at "Feenpalast 1" refrozen water was found near the base.

At the second location ("Feenpalast 2"), the ice appears mostly intransparent and has only thin layers of clear ice (Fig. 2g). Additionally, numerous thin sub-horizontal strata of a greyish to brownish particles are interposed. A similar stratum from Eisriesenwelt (see Sect. 4.3; May et al., 2011) was analyzed and found out to be cryogenic calcite (Spötl, 2008; Obleitner and Spötl, 2011). This form of calcite is produced by decarbonation when saturated water transforms to ice (Clarke and Lauriol, 1992). At the bottom, the ice transforms into an ice-debris mixture. A 12 m long profile was obtained at this location on a more than 9 m high ice cliff.

A 40 m long profile was measured at the nearby location "Saarhalle" which comprises an ice with a 40 m × 15 m wide planar surface (Fig. 2b). In September 2009 a 5.3 m long core was taken for isotopic analyses (Kern et al., 2011) at the deepest part of the profile. During the drilling small amounts of liquid water were extracted in depths between 3.3 and 3.6 m. Positive air temperatures (+0.3 °C) and thin (mm) layers of water were observed at several places on the ice surface. However, at the base melting of the ice was not observed.

4.2 Dachstein-Rieseneishöhle

Dachstein-Rieseneishöhle is located close to Dachstein-Mammuthöhle. Its passage length is only 2.7 km, but ice covers almost half of the cave. A 20 m long profile was recorded with a 200 MHz antenna on a 50 m × 30 m wide ice surface. The elevation of this location is 1460 m a.s.l. An outcrop in the anterior part gives a first idea of the possible ice thickness, as debris is partly exposed on the base and the maximum overall cave height is 20 m. In the vicinity of the profile, relatively large voids with sizes of 1 to 2 m are molten out by episodic water channels and air currents (Fig. 2f).

4.3 Eisriesenwelt

The Eisriesenwelt has an overall passage length of 42 km. The only known entrance is located 1642 m a.s.l., and the ice-covered part of the cave extends from there for almost 800 m. The "Eispalast" is an even ice surface at the end of the ice part with a slope of about 2°. It is 50 m × 8–20 m wide (1740 m a.s.l.). The ice temperatures close to the surface vary from $-1.5\,^{\circ}$C in late winter to $-0.3\,^{\circ}$C in summer. Three meters inside the ice, the temperature is about $-0.4\,^{\circ}$C throughout the year (Obleitner and Spötl, 2011).

4.4 Beilsteineishöhle

Beilsteineishöhle is located in the eastern part of the Northern Calcareous Alps at an elevation of 1330 m a.s.l. In contrast to the other ventilated caves, it represents a static ice cave. This type of ice caves exhibits only one (upper) entrance. Cold, dense air sinks down into the cave in winter and is conserved throughout the summer. If the amount of cold air is large enough, negative temperatures and cave ice can persist throughout the year. A 30 m long profile was recorded on a planar ice surface (1320 m a.s.l.).

5 Results

In the last chapter photographs of cave ice locations were introduced to show the visual outcrop of layers within the ice and to provide an impression of the diversity of the investigated ice. Here we present the unmigrated and migrated radargrams of all investigated locations, the cave ice structure and specific basal and internal reflection characteristics of the ice. Table 1 shows a summary of our result. This includes ice thickness and volume, visual inspections and reflection characteristics for the internal and basal structures for the investigated sites.

5.1 Dachstein-Mammuthöhle

At "Feenpalast 1" the base is clearly visible in form of a continuous reflector (Fig. 3a, b). Weak sub-horizontal layering

Table 1. Type, elevation, ice thickness and volume, visual inspections and reflection characteristics for the internal and basal structures for the investigated sites. The asterisk denotes locations where the calculation of the volume was not possible (irregular shape of the ice).

Location Elevation Ventilation type	Max. Thickness Volume	Internal reflections	Visual inspection of internal structures	Basal reflections	Visual inspection of basal structures	Wave speed ($m\,ns^{-1}$) Frequency (MHz)
Feenpalast 1 1360 m Dynamic	4 m ca. 940 m^3	Weak sub-surface parallel reflection bands	Diaphanous ice, slight stratification, low particle content	Sharp, reflective and continuous	Clay and debris (< 0.1m)	0.165 500
Feenpalast 2 1360 m Dynamic	>9 m not calculated*	Multitude of sharp, strong, reflection bands	Intransparent ice, strata with cryogenic calcites	Not observed	Debris-ice mixture	0.160 500
Saarhalle 1360 m Dynamic	6 m ca. 3200 m^3	Strong , sharp, subsurface parallel, tilted layers (6°)	Diaphanous ice	Large hyperbolae	Large boulders (1–2 m)	0.165 500
Rieseneishöhle 1460 m Dynamic	>15 m not calculated*	Large hyperbolae, few horizontal layers	Large voids (1–2 m), intransparent ice	Not clearly visible	Debris (<0.5 m)	0.160 200
Eisriesenwelt 1740 m Dynamic	7.5 m ca. 3700 m^3	Sharp, strong, tilted layers (3°), not sub-surface parallel	Not accessible	Small hyperbolae	Debris (0.5–1 m) in the E part	0.165 500
Beilsteineishöhle 1320 m Static	11 m ca. 4000 m^3	Zones of increased reflectivity, tilted layers (up to 10°)	Intransparent ice (outcrop beside the profile)	Highly reflective, continuous in the SE part	Sedimentary layer in the SE part	0.160 500

is seen above this reflector. Reflections from below the base are attributed to structures within the frozen sedimentary underground.

At "Feenpalast 2" the radargram section shows very pronounced layering of the ice (Fig. 3c, d). A multitude of reflection bands is visible down to depths of 4–6 m. The strata of two pronounced layers (Fig. 2d; presumably cryogenic calcite) correlate with reflectors in the GPR data (Fig. 3d).

At "Saarhalle" the maximum thickness of the ice is 6 m (Fig. 4). At one side it is possible to access the base at 4 m depth which is dominated by large boulders (average sizes of 1 to 2 m, Fig. 2b). Opposed to "Feenpalast 1 & 2", the radargram section does not yield a continuous reflector at the bottom, but represents a series of reflection hyperbolae with mean wave velocities of $0.165\,m\,ns^{-1}$. Remarkable features are multitudes of pronounced tilted reflection bands in the eastern and central part of the ice which are also visible on crossing profiles. The inclination of the internal layers is parallel to the base topography. Reflections from below the base are numerous and strong, and are attributed to either fissures in the bedrock or debris. We further find a shallow reflector (0.4 m to 1 m depth) in the eastern part.

5.2 Dachstein-Rieseneishöhle

The lower boundary of the ice is not clearly identifiable in the GPR data (Fig. 5), but the maximum thickness seems to be about 15 m. Between 3.5 and 5 m depth, short horizontal reflection bands can be identified. Compared to the radargrams from the other caves, reflection hyperbolae from within the ice are not associated with pronounced layering. The distinct reflection hyperbola at 80 ns and 13 m profile distance may results from an enclosed boulder.

5.3 Eisriesenwelt

Ice thickness in the eastern part ranges between 1.5 m and 2.5 m, while it rises to 7.5 m in the southern part (Fig. 6). The reflections from the base are characterized by numerous hyperbolae. In the shallow part, boulders with sizes ranging from 0.5 to 1 m are visible through the clear ice and it is likely that they account for the reflection hyperbolae. Again multitudes of slightly dipping reflection bands occur which traverse the entire ice. These well-visible layers can be identified down to 5 m depth. However, at this location the ice can't be accessed from the side. To ascertain the origin of

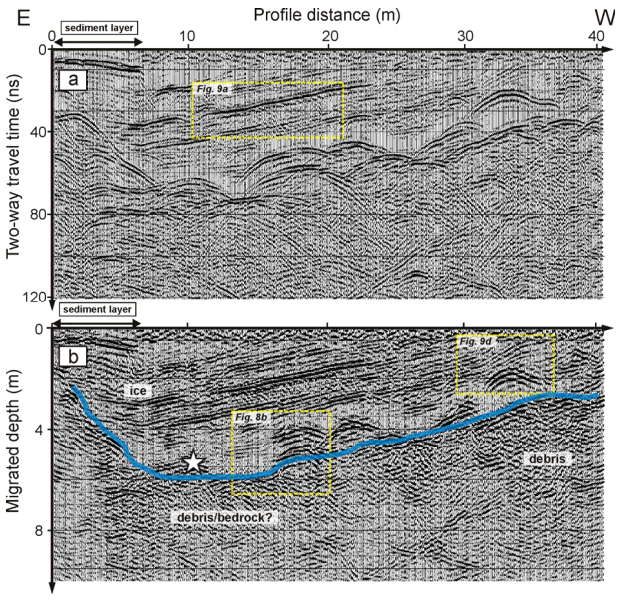

Fig. 4. Radargram section **(a)** from the location "Saarhalle" (Dachstein-Mammuthöhle). The white star indicates the maximum depth of a core drilling taken for isotopic analyses (Kern, 2011). The blue line in the migrated section **(b)** shows the interpreted base. Note the strong layering inside the ice in the uppermost 4 m and the marked visible shallow sediment layer (dipping from 0.4 to 1 m depth). Remarkable is the inclination of the internal layers which is parallel to the base topography. A picture of an outcrop which runs perpendicular to the GPR section at the profile distance of 30 m is shown in Fig. 2b.

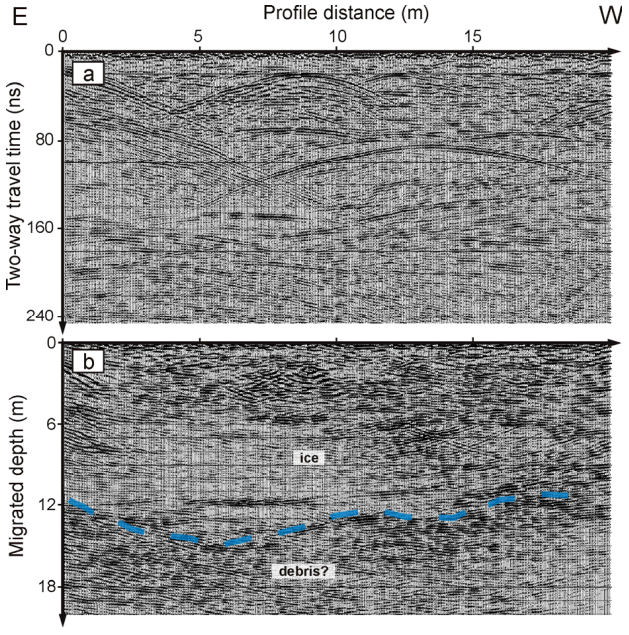

Fig. 5. Radargram sections **(a)** from Dachstein-Rieseneishöhle using the 200 MHz antenna. The base of the ice is better imaged in the migrated section **(b)**.

these reflections we compare the recorded data with synthetic data based on the results from the core drilling in the discussion (Sect. 6).

5.4 Beilsteineishöhle

The base is rather reflective in the right part and reveals a maximum ice thickness of about 10 m (Fig. 7). It is known from direct observation that the ice partly lies on a sediment layer. Further, in the south-eastern part the radargram appears relatively transparent in the upper 2 to 4 m and more reflective below. The reflections are characterized by both tilted layers and individual reflection hyperbolae. In contrast to the other caves, the layers are not as continuous.

5.5 Basal structure

Visual inspections of transition from the ice to the ground (Fig. 2) show that the base involves substrata such as sediment and debris (from fine-grained up to boulders of several meters in diameter). Massive bedrock was never encountered. In general, the base recorded by GPR is characterized by a sudden increase in reflectivity and termination of the internal layers (Fig. 8). The transition to a fine-grained

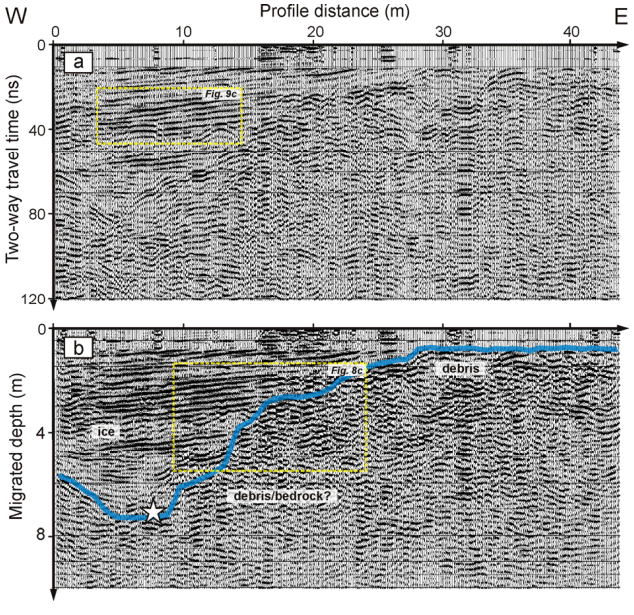

Fig. 6. Radargram section **(a)** from Eisriesenwelt. Note the strong layering in within the ice in the first half of the profile. The blue line in the migrated section **(b)** shows the interpreted base. The white star denotes the maximum ice depth (7.12 m) from the core drilling reported in May et al. (2011). Note that the inclination of the internal layers does not follow the base topography.

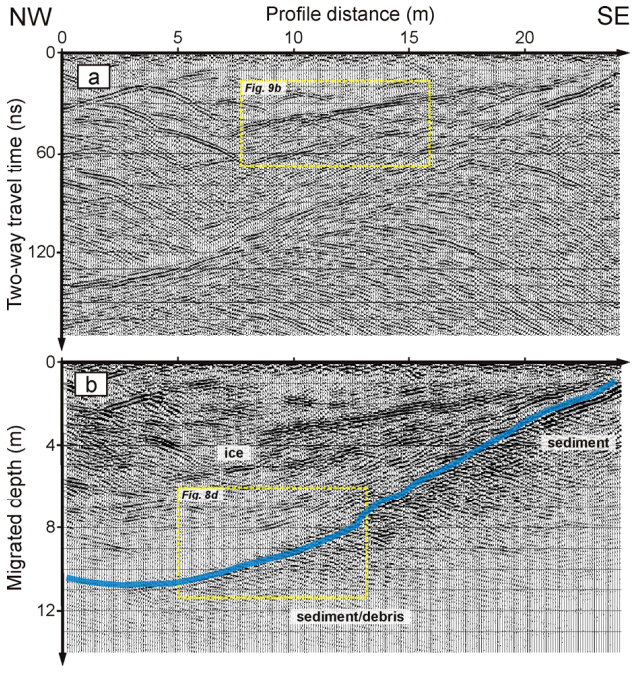

Fig. 7. Radargram section **(a)** from Beilsteineishöhle. The blue line in the migrated section **(b)** shows the interpreted base. In the right part pronounced internal reflections represent both tilted layers and individual reflection hyperbolae. The inclination of the reflection bands varies between almost horizontal and the slope of the interpreted base topography.

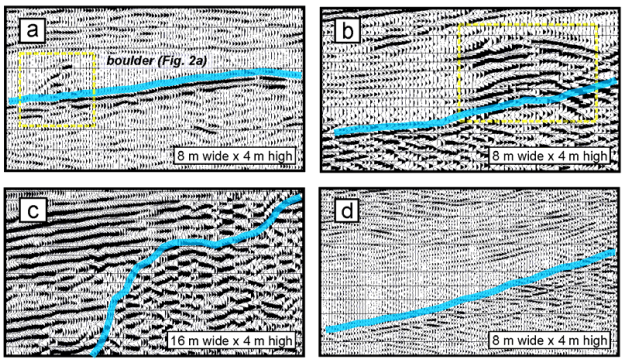

Fig. 8. Details from characteristic basal structures displayed as migrated sections. **(a)** Transition from ice to fine-grained sediment (Figs. 2a, 3). The reflective zone in the left part originates from a large boulder. **(b)** Transition from ice to either debris or jointed bedrock. The reflection signature is generated by large boulders (Fig. 2b). **(c)** The situation shown in Fig. 6 exhibits a base characterized by the termination of internal layers. The incoherent returns from the base originate from either debris or bedrock. **(d)** A base characterized by a sudden increase in reflectivity (see also Fig. 7). In the right part base parallel internal layers near the basal zone are visible.

sedimentary base is characterized by a short, high reflective, continuous reflector (Fig. 8a). The sediments are silts and clays with significantly higher permittivity than ice (Davis and Annan, 1989). Their origin is either dissolved limestone or remnants from glacial backfill. In contrast, a basal structure composed of large boulders (>0.5 m) is identified by a large number of high amplitude reflection hyperbolae (Fig. 4a, Fig, 8a, b). It must be considered that the contrast in permittivity is relatively small between ice (3–4) and limestone (4–8) (Davis and Annan, 1989). In this case, the strong amplitude of the reflections may be caused by increased humidity or voids between ice and debris.

5.6 Internal structure

Visual inspection of the ice in the Dachstein-Caves (Fig. 2) exhibit that fabrics (voids, particles, opaqueness) are significantly different at each location, and also change in vertical direction. Samples from the Dobsina ice cave (Clausen et al., 2007) reveal that intransparent, cloudy bands are caused by layers of small bubbles. They are the most common feature, but abundant brownish dark layers were also found. We also observe thin layers (up to 5 mm thickness) of particles (e.g. Fig. 2c). They most likely result from accumulation of cryogenic calcites (Clark and Lauriol, 1992) or dust resulting from "conventional" dissolution of limestone. In Eisriesenwelt embedded small boulders (up to 0.1 m in diameter) were found within the layers of the cryogenic calcites. The strata of the ice in "Feenpalast 2" (Fig. 2d) show changes of the temporal evolution of ice formation. Subsurface parallel strata in the footwall and horizontal strata in the hanging wall indicate that the run-off of the seepage water changed. In Rieseneishöhle large voids (>0.5 m, Fig. 2f) formed by episodic water channels and air currents were identified.

GPR images different internal reflection signatures from the ice (Fig. 9). Among them are tilted banded layers. Their inclination varies between horizontal and the slope of the sub-surface topography. The latter was observed at "Feenpalast 1" (Fig. 3b), at "Saarhalle" (Fig. 4b), and partially at the bottom at Beilsteineishöhle (Fig. 7b). At "Eispalast" (Fig. 6b) the layers are almost horizontal despite a strongly inclined subsurface topography.

At all locations reflections caused by point sources (e.g., small boulders) were found. They are either superimposed on the layers (Fig. 9) or occur as individual reflections. The point sources associated with layers are separated by regular and irregular intervals. Only at the location "Eispalast" the layers appear without point reflectors, but the termination of the layer is indicated by a pronounced diffraction hyperbola.

At the location "Saarhalle" a curved structure is observed (Fig. 9d). It is interpreted to be caused by subsurface undulation (e.g. a large boulder). Internal deformation of the ice would require a much higher load.

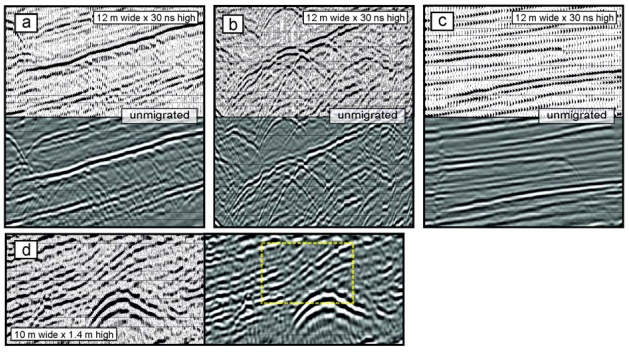

Fig. 9. Details from characteristic internal structures displayed in wiggle trace and variable density modus. **(a)** The detail of Fig. 4 shows many point sources at regular interval superimposed on the banded layers. **(b)** Much fewer point sources occur at irregular intervals on the detail from Fig. 7. **(c)** The layers appear without point reflectors, but the termination of a layer is indicated by a pronounced diffraction hyperbola (see Fig. 6). **(d)** The curved structure imaged in Fig. 4 probable originates from an underlain boulder.

6 Discussion

6.1 The electromagnetic wave speed

In this chapter we discuss the electromagnetic (EM) wave speed as well as the possible origin of the observed layering in the radargram sections. With regard to an uncertainty estimation, analyses of the EM wave speed and density data from the Eisriesenwelt ice core aim at calculating the volumetric amounts of air and liquid water in the ice.

The wave speed v ($\mathrm{m\,ns^{-1}}$) for any medium can be calculated from the permittivity ε' according to:

$$v = \frac{0.3}{\sqrt{\varepsilon'}} \quad (1)$$

For the permittivity of pure ice we use 3.2, which results in a velocity of $0.168\,\mathrm{m\,ns^{-1}}$ (Robin, 1975). The derived wave speeds are in the range from 0.160 to $0.165\,\mathrm{m\,ns^{-1}}$. The average from 6 locations is $0.163\,\mathrm{m\,ns^{-1}}$, which is lower than the wave speed for pure ice. Although the error analysis results in an accuracy of $\pm\,0.006\,\mathrm{m\,ns^{-1}}$ (Appendix A) the low average wave speed of $0.163\,\mathrm{m\,ns^{-1}}$ is significant since all obtained velocities are below $0.168\,\mathrm{m\,ns^{-1}}$. Looyenga's formula (Looyenga, 1965) enables to calculate the permittivity for mixed media, where it is assumed that both media are homogenously mixed. In reverse, when the permittivity and/or wave speed of the two constituting media are known, we can calculate their volumetric amounts in the mixture. To apply Looyenga's formula for a 3-phase media (ice, air and water or calcite powder) we used the extension presented in Heilig et al. (2009). In the following, we introduce permittivity values of 8 for calcite powder (Lebron et al., 2004), 80 for liquid water, and 1 for air.

Table 2. Liquid water and calcite content calculated from the observed EM wave speed and the mean density from the ice core at the location Eisriesenwelt.

	($\mathrm{m\,ns^{-1}}$)	volumetric content (%)	
	EM wave speed	water	calcite
maximum	0.169	0.6	3.4
mean	0.163	1.9	10.1
minimum	0.157	3.2	17.3

The investigation of a 7.12 m long ice core from Eisriesenwelt (May et al., 2011) led also to an estimate of the density (May, personal communication, 2010). The average density of the individual samples is $0.87 \pm 0.03\,\mathrm{g\,cm^{-3}}$ which is lower than the density of pure ice ($0.917\,\mathrm{g\,cm^{-3}}$, Andersland and Ladanyi, 2004). This could be explained by introducing a volumetric amount of 5% air which in turn would increase the wave speed to $0.172\,\mathrm{m\,ns^{-1}}$. In order to lower the wave speed to $0.163\,\mathrm{m\,ns^{-1}}$, we apply Looyenga's mixing formula again and estimate the corresponding volumetric amount of water and calcite powder (Table 2). With regard to the uncertainty analysis, we also consider a maximum velocity of $0.169\,\mathrm{m\,ns^{-1}}$ and a minimum wave speed of $0.157\,\mathrm{m\,ns^{-1}}$. It turns out that the occurrence of liquid water is more probable than the inclusion of calcite powder since the latter would require 10% of calcite powder. This would be in contradiction with the observed low density. On the other hand, the addition of 2% water would not change the density significantly. This assumption is supported by the fact that coring proved to be rather difficult: the 7.12 m long core was considerably fractured and broken up into more than 100 individual pieces. This could be explained by an increased presence of liquid water content in comparison to pure, cold ice.

6.2 The possible origin of the reflection bands

The discussion of the origin of the observed reflection bands in the GPR data addresses the following questions: (i) Do these reflections correlate with results from visual stratigraphy where available (Eisriesenwelt, "Feenpalast 2")? (ii) Could the accumulation of calcite cause these internal layers? (iii) Which are possible mechanisms for the formation of theses layers? Are they isochrones?

At first we qualitatively compared the observed reflection bands at Eisriesenwelt with the available data from the core drilling. The core was visually inspected for its stratification, and quasi-continuous depth profiles for gravimetric ice density, electrolytic conductivity and stable isotopes were performed in a laboratory (May et al., 2011). The visual inspection of the stratification showed a significant correlation with the GPR data. We also performed optical inspection of the

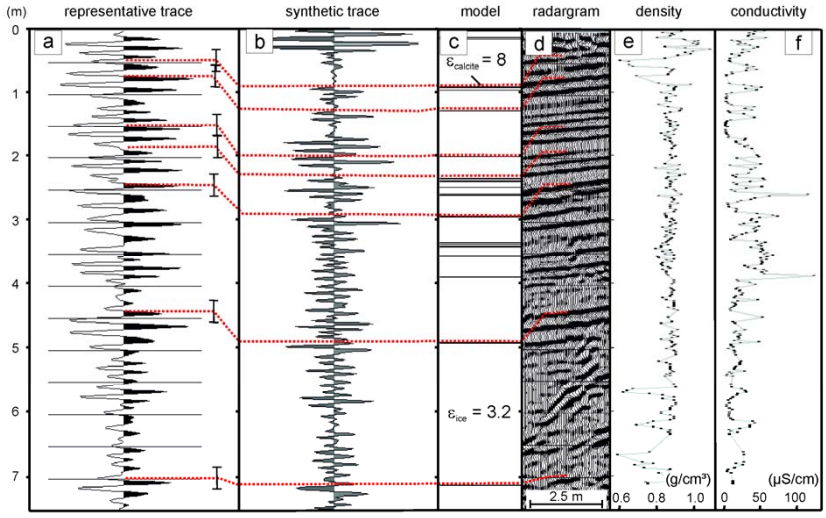

Fig. 10. Recorded reflection bands from GPR and synthetic data based on the interpreted layers of calcite powder from the core drilling (May et al., 2011) at the location Eisriesenwelt: **(a)** representative GPR signal (stacked from 10 individual traces), **(b)** synthetic signal, **(c)** GPR permittivity model, **(d)** recorded reflection bands, **(e)** density profile (May, personal communication, 2009), **(f)** electrolytic conductivity after May et al., 2010. The latter is shown for completeness. The red lines denote layers which produce significant reflections in the synthetic data and that can be correlated with (**a** and **d**). The error bars in **(a)** show the estimated uncertainty of the GPR signal.

ice cliff at the location "Feenpalast 2". Based on the obtained stratigraphy, we modelled the reflection bands by calcite layers in the ice.

To compare the synthetic data from a model with the recorded GPR data a representative trace was generated by stacking. At both locations the stacking was performed for single traces which were recorded within 0.5 m to the closest location of the visual stratigraphy. For the model we assume pure ice with layers of homogenously distributed calcite powder. Depth and thickness of these layers were obtained from the visual inspection of the stratification. For the simulation of the EM wave propagation we chose the FD-algorithm implemented in ReflexW, which is based on the solution of Maxwell equations. For the 2-D-model we used a center frequency of 500 MHz for the source wavelet (a Kuepper wavelet with a length of 2 ns), a sample interval of 0.008 m (in space) and 0.025 ns (in time), a range of 130 ns, as source the exploding reflectors, and linear absorbing-range as boundary condition. The physical parameters (permittivity, conductivity) are given in Table 3. For comparison we show the representative and the synthetic trace with the same gain as well as the model and the reflections bands. Where available we display a photograph of the visual inspection of the stratification and the density profile.

Figure 10 displays the comparison of the recorded reflection bands with synthetic data based on the stratification of the Eisriesenwelt core. Seven significant reflections from the synthetic data can be correlated with the representative trace from the GPR data. Out of these seven reflections, three high amplitude reflection bands (in 0.7, 2.4, and 4.4 m depth) can be clearly correlated with the modelled calcite layers. Some

Table 3. Physical parameters (permittivity, conductivity) which are used in the calculation of the synthetic traces.

	Permittivity ε'	Conductivity [µS m^{-1}]	Reference
Ice	3.2	9	Robin, 1975
Calcite powder	8.0	100	Lebron et al. (2004)

reflections in the synthetic data (e.g. in 5.7 m depth) do not originate from direct reflections of the calcite layers, but are identified to be multiple reflections.

The uncertainty of the wave speed (see error bars in Fig. 10a) is mostly smaller than the systematic shifts between the correlated field and synthetic data. Since the core has been extracted 3 m off-side the GPR profile, these systematic deviations are explained by the obliquity of the layers. The depth difference due to this dip can be estimated from an adjacent GPR profile and result in a value of about 0.25 m. This value is an additive factor, since the layers dip towards the borehole, and reduces the deviation for the correlated reflections significantly. With regard to this estimation we correlate the reflection bands with the calcite layers from the visual inspections of the Eisriesenwelt core.

For the location "Feenpalast 2" the stratification exhibits four pronounced sediment layers that were used for the generation of the synthetic model. Figure 11 shows the result of the synthetic data and the comparison with the representative trace from the recorded GPR data. High amplitude

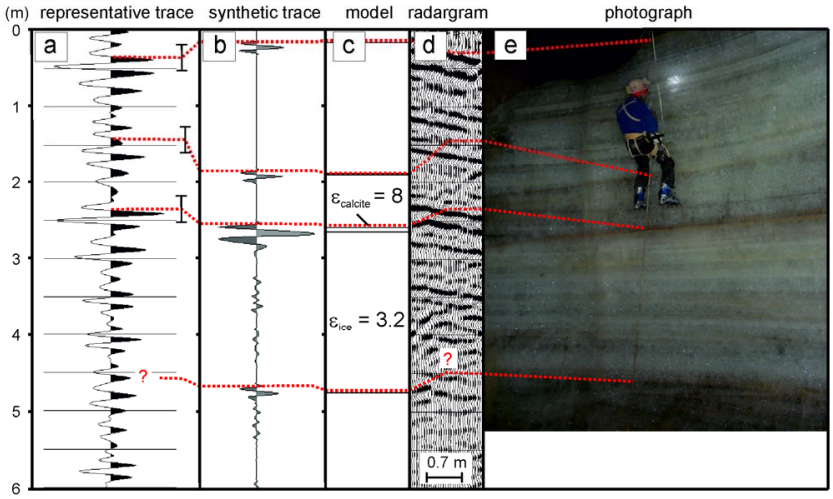

Fig. 11. Recorded reflection bands from GPR and synthetic data based on the interpreted layers of calcite powder from the strata taken at the location "Feenpalast 2" (Dachstein-Mammuthöhle): **(a)** representative GPR signal (stacked trace), **(b)** synthetic signal, **(c)** GPR model, **(d)** recorded reflection bands, **(e)** photograph. The red lines denote layers which produce significant reflections in the synthetic data and that can be correlated with (**a** and **d**). The error bars in **(a)** show the estimated uncertainty of the GPR signal.

reflections in a depth of 0.35 and 2.4 m can be correlated with the synthetic signal. Further, the most prominent sediment layer listed in the visual inspection of the stratification (in 2.6 m depth) produces a high amplitude reflection in the synthetic data which correlates clearly with a high amplitude reflection band. The correlation of the measured traces with the synthetic traces shows again different offsets and also different offset signs. We assume that an obliquely oriented inclination of the layers account for the different offsets. The different offset signs could be developed if the ice was first formed by seepage water and then by backwater. Such processes were interpreted in "Feenpalast 2" (Fig. 2d). However we suggest that dense layers of calcite powder produce high amplitude reflection bands in cave ice.

So far we showed that both of the inclusions (water, calcite) can be incorporated in the ice and that layer of calcite powder were presumably recorded as reflection bands by the GPR. The latter argumentation is strengthened by the observed lateral changes in amplitude along reflection bands (e.g. Figs. 3b, 7b) which are rather caused by interbedded particles with different grades of dispersal than by changes in the water content or changes in crystal-orientation fabric. Further this hypothesis is supported by the occurrence of reflections originating from a visible shallow sediment layer within the ice (Fig. 4). If we focus on the possible mechanism for the formation of these sediment layers we have to precede a period of ice degradation (MAAT $> 0\,^{\circ}$C) to generate layers of accumulated particles. These layers consist of particles (sediments in general, cryogenic calcites) and represent isochrones which are related to the onset of increased ablation Thus longer periods of degradation facilitates the formation of thicker layers that might be enriched with materials from above (e.g. small boulders). This can be observed at various locations (e.g. Eisriesenwelt; Spötl, 2008), and it could explain why several point sources were observed along such reflection bands. While at first sight the idea of isochrones seems plausible, the fact that some of them are tilted challenges this assumption. Possible mechanisms which are in accordance with the concept of isochrones and their tilted appearance may invoke run-off of seepage water or post-sedimentary basal melting, but this is subject to further studies. Wind action due to change in ventilation could cause the accumulation of these particles at the surface. The occurrence of the shallow reflector in the eastern part of "Saarhalle" is attributed to interbedded particles (presumably calcite powder), which are partially visible through the ice. This sediment layer and it's abrupt termination (Fig. 4a) might be explained by such processes.

7 Conclusions

GPR in combination with shielded antennae has been proven to be well suited to investigate the thickness and volume of the cave ice as well as to image their basal and internal structure. Centre frequencies between 200 and 500 MHz allow penetrating ice of at least 10–15 m thickness. The inferred ice thickness could be confirmed by core drilling (May et al., 2011; Kern et al., 2011) at the locations "Saarhalle" and "Eispalast". Like on glaciers (Eisen et al., 2003), the punctiform information gained from ice cores can be linked to the observation of continuous internal layers, and can thus be extended to wider areas.

Reflection signatures show that both basal and internal structure of the ice is far from being uniform. The continuity of basal reflections and/or the extent of associated reflection hyperbolae correlate with the deposit and the size of the underlying debris. Internal structure characterized by a multitude of pronounced tilted reflection bands were found at all locations. Stratigraphic sections, ice core data and synthetic GPR data were used to interpret the observed layering in the radargrams. This data show that the reflection bands can be correlated with the visual inspections of the stratification, and that layers of thin sediments could cause these reflections. The layers most likely result from accumulation of otherwise homogenously distributed particles (cryogenic calcites, or sediments in general) and are interpreted as isochrones (e.g. melting period).

Analysis of density and electromagnetic wave speed at one site suggests that the cave ice comprises an amount of about 5% air, and that the remaining mass is regarded as temperate ice with an liquid water content of about 2%.

Appendix A

Estimation of the accuracy of the wave speed

To determine the EM wave speed v the observed diffraction hyperbolas were used for the analyses. In order to define the accuracy of the wave speed we applied the analytical error propagation law. Therefore a functional relation between observables (apex and curvature of the hyperbolae) and unknown parameters (wave speed) has to be declared:

$$v = 2 \cdot \sqrt{\frac{(x_0 + \Delta x)^2 - x_0^2}{(t_0 + \Delta t)^2 - t_0^2}} \tag{A1}$$

The parameters x_0 and t_0 define the apex of the hyperbolae, Δx is the distance ranging from the apex to a user-specific point, Δt is the time span between the apex and a user-specific point and $x_0 + \Delta x$, $t_0 + \Delta t$ define a user-specific point of the hyperbolae. To calculate the standard deviation of the wave speed we used the covariance propagation law (e.g. Mikhail, 1976; Reissmann, 1976):

$$\Sigma_{yy} = \mathbf{A} \cdot \Sigma_{xx} \cdot \mathbf{A}^T \tag{A2}$$

It uses the functional matrix $\mathbf{A}$ (Jacobi matrix) and the covariance matrix Σ_{xx}. The elements of matrix $\mathbf{A}$ contain the first derivative of each observation with respect to Eq. (A1) and the matrix Σ_{xx} contains all variances of the observations. The standard deviation of the unknown parameters is obtained in Σ_{yy}. We analysed three representative hyperbolas located at the base of the ice in Dachstein-Mammuthöhle and Beilsteineishöhle. Using standard deviations of ± 0.02 m for errors in the geometry and ± 1 ns for errors in the time domain we obtain an error of $\pm 0.006\,\mathrm{m\,ns^{-1}}$ for the identification of an individual hyperbolae.

Acknowledgements. Thanks go to the owners and operators of the caves (Fritz Oedl Oedl, Austrian Federal Forestry AG, Stephan Höll, Alois Rettenbacher) for their support and collaboration. Furthermore, we would like to thank all other staff at the caves and everyone who helped out during the surveys. Joanneum Research contributed towards the study by supplying the 200 and 400 MHz antennae. The dedication shown by Daniel Binder allowed efficient conduction of the GPR surveys and was also particularly helpful during the processing. The measurements and data interpretation were sponsored by the Austrian Academy of Sciences as part of the AUSTRO ICE CAVES 2100 project. We further thank Barbara May (Heidelberg University, Germany) and Zoltan Kern (Hungarian Academy of Sciences) for providing information on the ice core data. Photographs were kindly provided by Andreas Neumann, Gernot Weyss, and Robert Illnar. We acknowledge the comments of Olaf Eisen (Alfred Wegener Institute) and the anonymous reviewer that helped to significantly improve the manuscript.

Edited by: M. Luetscher

References

Achleitner, A.: Zum Alter des Höhleneises in der Eisgruben-Eishöhle im Sarstein (Oberösterreich). Die Höhle – Fachzeitschrift für Karst- und Höhlenkunde, 46(1), 1–5, 1995.

Andersland, O. B. and Ladanyi, B.: Frozen Ground Engineering, Second edition, 363 pp., JohnWiley & Sons Inc., 2004.

Arcone, S. A., Lawson, D. E., and Delaney, A. J.: Short-pulse radar wavelet recovery and resolution of dielectric contrasts within englacial and basal ice of Matanuska Glacier, Alaska, USA, J. Glaciol., 41(137), 68–86, 1995.

Behm, M. and Hausmann, H.: Eisdickenmessungen in alpinen Höhlen mit Georadar. Die Höhle - Fachzeitschrift für Karst- und Höhlenkunde, 1–4(58), 3–11, 2007.

Behm, M. and Hausmann, H.: Determination of ice thicknesses in alpine caves using georadar, in: Proceedings of the 3rd International Workshop on Ice Caves, edited by: Kadebskaya, O., Mavlyudov, B. R., and Pyatunin, M., Kungur, Russia, 70–74, 2008.

Binder, D., Brückl, E., Roch, K. H., Behm, M., and Schöner, W.: Determination of total ice volume and ice thickness distribution of two glaciers in the Hohen Tauern (Eastern Alps) by ground penetrating radar (GPR). Ann. Glaciol., 50(51), 71–79, 2009.

Bingham, R. G. and Siegert, M. J.: Radio-Echo Sounding Over Polar Ice Masses, J. Environ. Eng. Geoph., 12(1), 47–62, doi:10.2113/JEEG12.1.47, 2007.

Cigna, A. A.: Climate of caves, in: Encyclopedia of caves and karst science, edited by: Gunn, J., Fitzroy Dearbon, New York, 229–230, 2004.

Clarke, I. D. and Lauriol, B.: Kinematic enrichment of stable isotopes in cryogenic calcites, Chem. Geol. (Isotope Geoscie. Sect.), 102, 217–228, 1992.

Clausen, H. B., Vrana, K., Hansen, S. B., Larsen, L. B., Baker, J., Siggaard-Andersen, M. L., Sjolte, J., and Lundholm, S. C.: Continental ice body in Dobsina Ice Cave (Slovakia) – Part II. – Results of chemical and isotopic study, in: Proceedings of the 2nd International Workshop on Ice Caves, edited by: Zelinka, J., Demanovska Dolina, Slovak Republic, 29–37, 2007.

Davis, J. L. and Annan, A. P.: Ground penetrating radar for high resolution mapping of soil and rock stratigraphy, Geophs. Prospect., 37, 531–551, 1989.

Delaloye, R. and Lambiel, C.: Evidences of winter ascending air circulation throughout talus slopes and rock glaciers situated in the lower belt of alpine discontinuous permafrost (Swiss Alps), Norsk Geogr. Tidsskr., 59, 194–201, 2005.

Eisen, O., Nixdorf, U., Wilhelms, F., and Miller, H.: Electromagnetic wave speed in polar ice: Validation of the CMP technique with high resolution dielectric-profiling and gamma-density measurements, Ann. Glaciol., 34, 150–156, 2002.

Eisen, O., Wilhelms, F., Nixdorf, U., and Miller, H.: Revealing the nature of radar reflections in ice: DEP-based FDTD forward modeling, Geophys. Res. Lett., 30(5), 1218, doi:10.1029/2002GL016403, 2003.

Eisen, O., Hamann, I., Kipfstuhl, S., Steinhage, D., and Wilhelms, F.: Direct evidence for continuous radar reflector originating from changes in crystal-orientation fabric, The Cryosphere, 1, 1–10, doi:10.5194/tc-1-1-2007, 2007.

Fukui, K., Sone, T., Strelin, J. A., Torielli, C. A., Mori, J., and Fujii, Y.: Dynamics and GPR stratigraphy of a polar rock glacier on James Ross Island, Antarctic Peninsula, J. Glaciol., 54(186), 445–451(7), 2008.

Geczy, J. and Kucharovic, L.: Determination of the ice filling thickness at the selected sites of the Dobsinska ice cave (in slovak, engl. summary). Ochrana ladovych jaskyn Zilina: 17–23, 1995.

Gudmandsen, P.: Layer echos in polar ice sheets, J. Glaciol., 15(73), 95–101, 1975.

Harrison, C. H.: Radio echo sounding of horizontal layers in ice, J. Glaciol., 12(66), 383–397, 1973.

Heilig, A., Schneebeli, M., and Eisen, O.: Upward-looking ground-penetrating radar for monitoring snowpack stratigraphy, Cold Reg. Sci. Technol., 59, 152–162, 2009.

Katsube, T. V., Wadleigh, M., and Erickson, R.: Electrical properties of permafrost samples, Geol. Surv. Can. Paper, 76–1C, 83–90, 1976.

Kern, Z., Fórizs, I., Pavuza, R., Molnár, M., and Nagy, B.: Isotope hydrological studies of the perennial ice deposit of Saarhalle, Mammuthöhle, Dachstein Mts, Austria, The Cryosphere, 5, 291–298, 2011,
http://www.the-cryosphere-discuss.net/5/291/2011/.

Lebron, I., Robinson, D. A., Goldberg, S., and Lesch, S. M.: The Dielectric Permittivity of Calcite and Arid Zone Soils with Carbonate Minerals, Soil Sci. Soc. Am. J., 68, 1549–1559, 2004.

Looyenga, H.: Dielectric constants of heterogeneous mixtures, Physica, 31, 401–406, 1965.

Luetscher, M.: Processes in ice caves and their Significance for Paleoenvironmental Reconstructions, Phd-thesis, Universität Zürich, Swiss Institute for Speleology and Karst Studies (SISKA), 2005.

May, B., Spötl, C., Wagenbach, D., Dublyansky, Y., and Liebl, J.: First investigations of an ice core from Eisenriesenwelt cave (Austria), The Cryosphere, 5, 81–93, 2011,
http://www.the-cryosphere-discuss.net/5/81/2011/.

Mikhail, E. M.: Observations and least squares. IEPA Dun-Donnelley, New York, 1976.

Novotny, L. and Tulis, J.: Ice filling in the Dobsina ice cave, Kras a jaskyne (Liptovsky Nikulas) 16–17, 1995.

Obleitner, F. and Spötl, C.: The mass and energy balance of ice within the Eisriesenwelt cave, Austria, The Cryosphere, 5, 245–257, 2011,
http://www.the-cryosphere-discuss.net/5/245/2011/.

Phillips, M., Mutter, E. Z., Kern-Luetschg, M., and Lehning, M.: Rapid degradation of ground ice in a ventilated talus slope: Flüela Pass, Swiss Alps, Permafrost Periglac., 20(1), 1–14, 2009.

Podsuhin, N. and Stepanov, Y.: Measuring of the thickness of perennial ice in Kungur Ice Cave by georadar, in: Proceedings of the 3rd International Workshop on Ice Caves, edited by: Kadebskaya, O., Mavlyudov, B. R., Pyatunin, M., Kungur, Russia, 52–55, 2008.

Reissmann, G.: Die Ausgleichungsrechnung, Grundlagen und Anwendung in der Geodäsie, 5. Auflage, VEB Verlag fr Bauwesen, Berlin, 1976.

Robin, G. D. Q., Evans, S., and Bailey, J. T.: Interpretation of Radio Echo Sounding in Polar Ice Sheets, Phil. Trans. R. Soc. Lond., A December 18, 1969 265, 437–505, doi:10.1098/rsta.1969.0063, 1969.

Scott, W. J., Sellmann, P., and Hunter, J. A.: Geophysics in the study of permafrost. In Geotechnical and Environmental Geophysics, Vol. 1: Review and Tutorial, Society of Exploration Geophysicists Investigation in Geophysics no. 5, 355–38, 1990.

Siegert, M.: On the origin, nature and uses of Antarctic ice-sheet radio-echo layering, Prog. Phys. Geogr., 23, 159–179, 1999.

Spötl, C.: Kryogene Karbonate im Höhleneis der Eisriesenwelt (Cryogenic carbonates in cave ice of the Eisriesenwelt). In german, english summary. Die Höhle – Fachzeitschrift für Karst- und Höhlenkunde, 59(1–4), 26–36, 2008.

Stummer, G. and Plan, L.: Handbuch zum Österreichischen Höhlenverzeichnis (Documenation for the Austrian cave cadastre). Speldok, Verb. Österr. Höhlenforscher, Wien, 2002.

Wimmer, M.: Eis- und Lufttemperaturmessungen im Schönberg-Höhlensystem (1626/300) und Modellvorstellungen über den Eiszyklus. (Ice and air temperature measurements in the Schönberg-Höhlensystem (Totes Gebirge, Austria) and a model of cyclic ice dynamics). In german, english summary. Die Höhle, 59, 1–4, 13–25, 2008.

Yilmaz, Ö.: Seismic data analysis, 2nd edition, Society of Exploration Geophysicists, 2001.

Yonge, C. J.: Ice in caves, in: Encyclopedia of caves and karst science, edited by: Gunn, J., Fitzroy Dearbon, New York, 435–437, 2004.